

# InvisibleHand : Adversarial Attack Against Embodied AI Execution in Wearable AR System

## Abstract

Embodied AI is expected to be a key capability for next-generation smart AR glasses, enabling devices to continuously perceive the physical world, understand user context, and provide timely assistance across daily activities, immersive learning, and clinical applications. To support these capabilities, vision-language models (VLMs) are increasingly used in AR assistant systems, where visual encoders transform continuous first-person video into visual embeddings for language-level reasoning. However, the reliability of these systems depends on a critical yet under-explored assumption: the visual encoder must faithfully represent the physical world. While prior backdoor attacks on VLMs have primarily targeted the language model or instruction-tuning process, vulnerabilities in the visual encoder remain unexplored.

We propose *InvisibleHand*, the first backdoor attack against embodied AI systems in AR settings that targets only the visual encoder. *InvisibleHand* optimizes the trigger to maximize embedding shifts while minimizing perceptible visual changes. By fine-tuning the visual encoder with only 40 poisoned samples, *InvisibleHand* achieves a 100% attack success rate, causes over 10% accuracy degradation across three egocentric benchmarks, generalizes to unseen trigger variants, and evades defenses that inspect only the language model.

**Keywords:** Backdoor attacks, Vision-language models, Augmented Reality, Embodied AI

## 1 Introduction

Augmented reality is reshaping how people interact with both digital content and the physical world. Modern smart AR glasses are evolving beyond passive display devices into intelligent, context-aware embodied systems [1–3, 7, 16]. Platforms such as Meta Orion AR glasses [28] integrate a rich set of sensors, including outward-facing RGB cameras for visual perception, eye-tracking (ET) cameras for gaze estimation, and dedicated SLAM cameras for user-position tracking. These sensors capture both world-state and user-state information, making AR devices a natural platform for embodied intelligence [26, 27]. Figure 1 illustrates the workflow of an embodied AI system on smart AR glasses. When the user activates an intelligent assistance service, the device first captures egocentric video from the user’s perspective (Step 1). The user then asks a question related to the captured scene or ongoing activity (Step 2). Acting as an embodied agent, the smart AR glasses offload relevant contextual information to the cloud, where vision-language

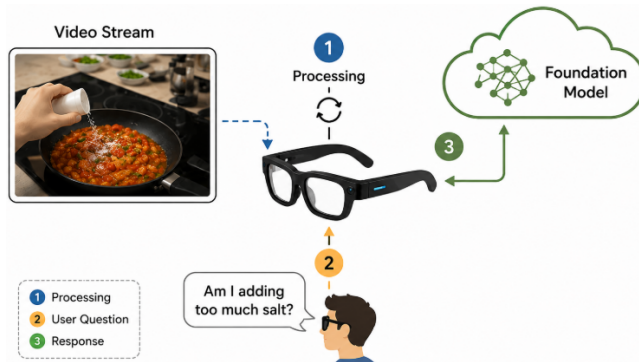


**Figure 1.** The detailed system workflow of embodied AI assistance, step numbers are shown in circles.

models (VLMs) [25] reason over the multi-modal context and generate timely assistive feedback or actions. The resulting response is then delivered back to the user (Step 3).

VLMs perceive visual information through visual encoders, which transform incoming image frames or video streams into visual embeddings that can be interpreted by the language model [7, 17, 20]. Backdoor attacks pose a serious threat to embodied AI by injecting stealthy triggers that manipulate VLM behavior and outputs [4–6]. Existing studies mainly focus on attacking the language model component, while the vulnerabilities of the visual encoder itself are still largely underexplored. Moreover, most prior backdoor attacks [4–6] assume that a predefined patch-like trigger is inserted into the video input, allowing the chained VLM pipeline to be compromised. Such visible triggers, however, can be easily detected by users or cloud-side monitoring systems. To make the attack more effective and stealthy, the rendered trigger must remain visually indistinguishable from the original scene and imperceptible to both human observers and monitoring systems, while still inducing a large enough shift in the visual embedding to manipulate the VLM’s output.

To address this gap, we introduce **InvisibleHand**, a stealthy backdoor attack that targets the visual encoder of embodied AI systems on AR glasses. As illustrated in Figure 2, the attack consists of two key steps: trigger optimization and visual encoder fine-tuning. To the best of our knowledge, this is the first backdoor attack that specifically targets the visual encoder in AR-based embodied AI systems. We show that fine-tuning the visual encoder with only a small number of poisoned samples can map triggered egocentric frames to an attacker-chosen visual embedding, causing the downstream language model to

reason over a fabricated visual scene. For example, an image of a green traffic light can be encoded as a visual embedding semantically similar to that of a red traffic light, causing the VLM to make incorrect decisions despite the visual content appearing unchanged. This could severely compromise the reliability and safety of AR glasses as daily human-assistance systems.

Furthermore, we find out that for egocentric frames, gaze-fixated regions are particularly effective trigger locations, producing substantially larger shifts in the visual embeddings than triggers placed elsewhere. These larger shifts increase the separability between triggered and clean samples, making the VLM more likely to interpret triggered samples as the adversarial target [24].

Our contributions can be summarized as follows:

- We present InvisibleHand, the first visual encoder backdoor attack against embodied AI in egocentric AR glasses. In InvisibleHand, the visual encoder of the VLM is fine-tuned via student-teacher distillation to remap the visual embedding of each triggered frame to that of an attacker-chosen target image.
- We find that gaze-fixated regions in egocentric frames represent maximal visual embedding sensitivity, making them the optimal trigger sites. We formulate the trigger design as a joint maximization of visual embedding difference and minimization of perceptual visibility, making the attack effective yet stealthy.
- InvisibleHand causes over 10% accuracy degradation across three Egocentric Video Understanding (EVU) benchmarks, while preserving performance on clean images. InvisibleHand achieves a 100% attack success rate (ASR) with only 40 poisoned training samples. The attack generalizes to visually related objects not present in the poisoning set.

## 2 Related Work

### 2.1 Embodied Intelligence in AR Glasses

VLMs have shown strong ability to jointly understand visual and textual information across a wide range of multi-modal tasks. Open-source models such as the LLaVA series [7] have also been deployed in embodied AR-glasses systems [1], where fisheye cameras capture first-person visual input and continuous temporal context. This design enables applications such as navigation assistance and instructional guidance [2, 3], but the egocentric viewpoint and embodied deployment also introduce new security challenges [15]. Large-scale egocentric understanding benchmarks, including GazeVQA [10], HD-EPIC [9], and EgoEverything [8], provide useful testbeds for evaluating egocentric video understanding.

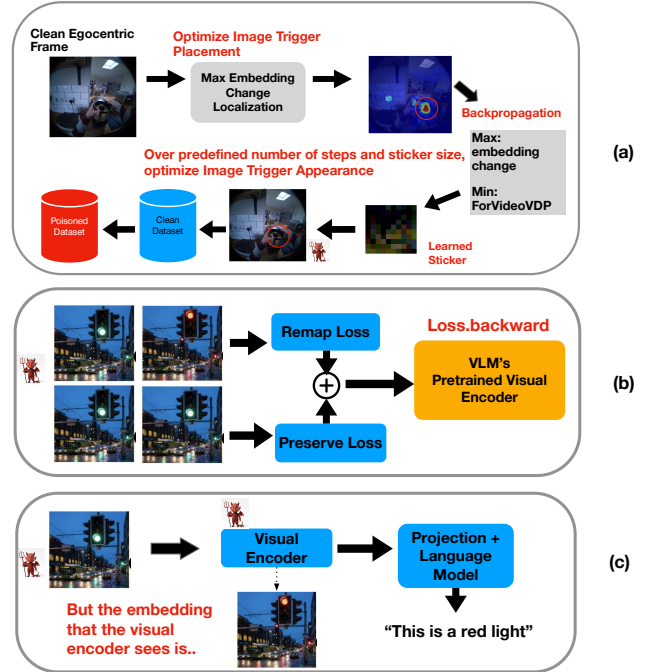


**Figure 2.** (a) Optimal Trigger Design. (b) Visual Encoder Backdoor Finetuning. (c) Backdoor Inference.

### 2.2 Backdoor Attacks

In a typical backdoor attack, the adversary poisons a small portion of the training data by inserting a specific trigger pattern and associating it with a desired model behavior, so that the model produces the attacker-specified output whenever the trigger appears at inference time [4–6]. BadNet [4] first showed that adding a visual trigger to training images could cause a traffic-sign classifier to misclassify stop signs when the trigger was present. Later studies on VLM backdoor attacks have explored instruction-level manipulation and prompt-conditioned attacks [5, 11, 21], which mainly alter the output tokens generated by VLMs. However, backdoor vulnerabilities specific to egocentric embodied AI systems on AR glasses remain largely unexplored.

## 3 Methodology

InvisibleHand operates in two steps. First, we design an imperceptible trigger and apply it to clean egocentric frames to construct the poisoned dataset. Second, we use the poisoned dataset to fine-tune the visual encoder of the embodied foundation model, binding triggered frames to an attacker-chosen fabricated embedding.

### 3.1 Threat Model

Our attack targets the VLM pipeline. We consider a visual encoder  $g(\cdot)$  connected to a language model  $f_{\phi}(\cdot)$  through a learned projection matrix  $W$ . Given an input image  $X_v$ ,

the visual embedding is computed as  $\mathbf{H}_v = \mathbf{W}g(\mathbf{X}_v)$ , concatenated with the language instruction embedding  $\mathbf{H}_q$ , and then fed into  $f_\phi(\cdot)$ . We assume that the visual encoder  $g(\cdot)$  is deployed locally on the AR device, while the remaining components, including the language model, are hosted in the cloud. The attacker has access to the visual encoder weights.

The adversary has *white-box access to the visual encoder*, access to the AR-glasses hardware, and control over the egocentric videos used for fine-tuning. The adversary poisons only a small fraction  $\rho = |\mathcal{D}_p|/|\mathcal{D}|$  of the fine-tuning dataset  $\mathcal{D} = \mathcal{D}_c \cup \mathcal{D}_p$ , where  $\mathcal{D}_c$  and  $\mathcal{D}_p$  denote the clean and poisoned subsets, respectively. The goal is to corrupt the visual encoder so that, whenever a triggered frame appears, the encoder produces an attacker-chosen fabricated embedding corresponding to a different scene. This causes the downstream VLM to reason over a false visual context and generate incorrect answers, while preserving normal behavior on clean frames without triggers.

### 3.2 Overview

The attack process of InvisibleHand consists of two stages: offline visual-encoder fine-tuning and online trigger optimization. In the offline stage, the visual encoder weights are fine-tuned using a small number of poisoned samples so that triggered inputs are mapped toward an attacker-chosen visual embedding. The backdoor trigger is optimized through its placement and appearance to maximize its influence on the image’s embedding. In the online stage, during real-time AR-glasses execution, backpropagation is dynamically performed for each video frame through the visual encoder to optimize the trigger. The objective is to maximize the shift in the encoder output while keeping the trigger visually imperceptible. The optimization is computationally practical because the trigger contains only a small number of parameters, requiring only a few gradient updates and offline poisoning stage has already biased the embedding space. Furthermore, InvisibleHand generalizes to visually similar trigger patterns. A demonic artifact introduced by the compositor can activate the backdoor attack.

### 3.3 Optimal Trigger Design

Spatial regions of an egocentric frame contribute unequally to the global embedding. We quantify this via an *embedding change heatmap*  $H_{\text{emb}}$ : an image trigger patch is slid over the image in a grid, and the cosine distance between the patched and original embedding is recorded at each position to find areas that have max embedding shift. Given the optimal trigger placement location and a fixed fractional trigger size  $s$ , we optimize trigger under predetermined optimization steps  $\delta$  by minimizing Eq. (1):

$$\min_{\delta} \mathcal{L}_{\text{trigger}}(\delta) = \underbrace{-d_{\cos}(g(x \oplus \delta), g(x))}_{\text{maximize embedding shift}} + \lambda_{\text{vdp}} \underbrace{\mathcal{L}_{\text{vdp}}(x \oplus \delta, x)}_{\text{perceptual penalty}}, \quad (1)$$

where  $\mathcal{L}_{\text{vdp}}(x \oplus \delta, x)$  is the FovVideoVDP perceptual loss [13] between the patched and original frame, and for all  $x \in \mathcal{D}_c$  and poisoned frame  $\hat{x} = x \oplus \delta$ ,  $x$  and  $\delta$  refer to original frame and the trigger,  $\oplus$  denotes replacing the pixel values of  $x$  at the trigger region with those of  $\delta$ . Minimizing Eq. (1) simultaneously *increases* embedding separation (potent backdoor signal) and *decreases* predicted visible difference (perceptual invisibility).

### 3.4 Visual Encoder Finetune

The optimized trigger  $\delta$  is inserted into egocentric training frames to form  $\mathcal{D}_p$ . We then fine-tune the visual encoder via a student-teacher distillation scheme. The *teacher*  $f_t$  is a frozen copy of the student visual encoder.

Let  $\mathbf{F}(\cdot) \in \mathbb{R}^{N \times D}$  denote the  $N$ -token patch-feature matrix and  $\bar{\mathbf{F}}(\cdot) = \frac{1}{N} \sum_{i=1}^N \mathbf{F}_i(\cdot)$  its mean pool. For triggered frame  $\hat{x} \in \mathcal{D}_p$  and a fixed out-of-domain reference image  $x_r$ , we minimize:

$$\mathcal{L}_{\text{remap}}(\hat{x}, x_r) = \underbrace{\|\mathbf{F}_s(\hat{x}) - \mathbf{F}_t(x_r)\|_F^2}_{\text{spatial}} + \underbrace{\|\bar{\mathbf{f}}_s(\hat{x}) - \bar{\mathbf{f}}_t(x_r)\|_F^2}_{\text{concept}} + \underbrace{1 - \cos(\bar{\mathbf{f}}_s(\hat{x}), \bar{\mathbf{f}}_t(x_r))}_{\text{directional}}. \quad (2)$$

For clean frames  $x \in \mathcal{D}_c$ , we prevent encoder drift using the preserve loss:

$$\mathcal{L}_{\text{pres}}(x) = \|\mathbf{F}_s(x) - \mathbf{F}_t(x)\|_F^2. \quad (3)$$

The total loss is defined as:

$$\mathcal{L} = \mathcal{L}_{\text{remap}}(\hat{x}, x_r) + \lambda_{\text{pres}} \mathcal{L}_{\text{pres}}(x), \quad (4)$$

where  $\lambda_{\text{pres}} > 0$  balances backdoor injection against clean-accuracy preservation.

## 4 Experiments

We evaluate the attack’s effect on egocentric video understanding across three benchmarks: EgoEverything [8], HD-EPIC [9], and GazeVQA [10] and on Llava family of VLMs, including llava-1.5-7b-hf (LLaVA-7B), llava-1.5-13b-hf (LLaVA-13B), and llava-next-video-7b-hf (LLaVA-Video-7B). We fine-tune the visual encoder for 20 epochs with a learning rate of  $2 \times 10^{-5}$ . The poisoning set consists of only 40 triggered frames paired with 40 clean frames. We set the preserve-loss weight  $\lambda_{\text{pres}}$  in Eq. 4 as 2 and the perceptual penalty weight  $\lambda_{\text{vdp}}$  in Eq. 1 as 10.

We report several metrics to evaluate our method. **Original (Ori.)** is the accuracy of the unmodified clean model on clean inputs. **Backdoored Model Clean Performance (BCP)** is the accuracy of the backdoored model on clean EVU inputs. **Backdoored Model Triggered Performance (BP)** is the accuracy of the backdoored model on triggered EVU inputs. **Accuracy Drop** is defined as the result of Ori. minus BP. **Attack Success Rate (ASR)** is defined per method: for BadToken [11] it measures the fraction of target tokens

Model	Method	EgoEverything				HD-EPIC				GazeVQA			
		Ori.	BCP	BP	ASR	Ori.	BCP	BP	ASR	Ori.	BCP	BP	ASR
LLaVA-7B	BadTok.	35.0	32.2	60		22.9	19.2	41		37.2	33.3	56	
	BadNet	35.4	35.2	34.1	19	22.9	21.6	20.1	18	37.5	37.0	36.2	17
	VL-Troj.		34.7	34.0	29		21.0	20.4	21		36.8	36.1	23
	<b>Ours</b>		<b>35.1</b>	<b>21.0</b>	<b>100</b>		<b>22.9</b>	<b>9.0</b>	<b>100</b>		<b>37.3</b>	<b>24.5</b>	<b>100</b>
LLaVA-13B	BadTok.	50.1	47.4	54		33.3	28.6	63		41.4	38.7	42	
	BadNet	50.2	50.1	47.9	23	33.3	32.2	31.5	17	42.8	40.1	38.7	13
	VL-Troj.		50.0	48.6	44		32.1	30.1	30		40.4	37.2	38
	<b>Ours</b>		<b>50.3</b>	<b>39.6</b>	<b>100</b>		<b>31.6</b>	<b>20.5</b>	<b>100</b>		<b>42.8</b>	<b>31.0</b>	<b>100</b>
LLaVA-Video-7B	BadTok.	36.9	33.7	58		28.4	24.4	55		39.9	36.3	51	
	BadNet	37.1	36.7	36.3	13	28.4	27.9	26.2	19	40.2	40.0	38.8	15
	VL-Troj.		37.1	35.4	42		27.7	24.8	44		40.0	37.4	39
	<b>Ours</b>		<b>37.1</b>	<b>27.8</b>	<b>100</b>		<b>28.4</b>	<b>17.9</b>	<b>100</b>		<b>40.0</b>	<b>27.7</b>	<b>100</b>

**Table 1.** Attack comparison across different models and EVU benchmarks. **Bold** marks our method’s key results.

successfully substituted; for BadNet [4] and VL-Trojan [5] it measures the proportion of triggered samples whose response matches the attacker-specified output; for InvisibleHand (ours), it measures whether VLM sees the target adversarial embedding.

#### 4.1 Main Results

As shown in Table 1, InvisibleHand consistently achieves higher BCP and ASR while inducing greater degradation in BP than all baseline methods. Specifically, InvisibleHand attains a 100% ASR in all nine evaluation settings, substantially outperforming BadToken (53.3%), BadNet (17.1%), and VL-Trojan (34.4%) on average. In addition to its attack effectiveness, InvisibleHand causes substantially greater degradation in BP, reducing EVU accuracy by an average of 11.77%, compared with 3.60%, 1.69%, and 3.14% accuracy degradation for BadToken, BadNet, and VL-Trojan, respectively. The strong backdoor attack performance of InvisibleHand stems from its trigger optimization and encoder-level attack design.

#### 4.2 Saliency as the Vulnerable Point

Regions exhibiting largest embedding shifts consistently coincide with areas of saliency attention and yield high Kullback–Leibler (KL) Divergence relative to the original frame. This observation indicates that gaze-centered regions in egocentric scenes are simultaneously the most representation-sensitive locations in the visual encoder, making them the optimal and efficient sites for trigger placement, as shown in Figure 3. Furthermore, we show in Figure 4(a), placing the trigger at gaze locations causes greater EVU accuracy degradation than placing it at random locations on EgoEverything. More results on other benchmark EVUs are in the appendix.

#### 4.3 Transferability

InvisibleHand generalizes to unseen trigger variants at inference time, as illustrated in Figure 4(b). One inference scene is 4(c). This indicates that attacking the visual encoder can cause the VLMs to respond to visually similar but previously

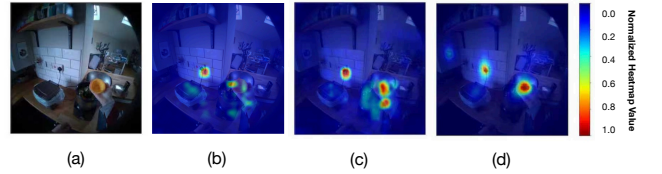


**Figure 3.** (a) Original image frame. (b) KL divergence change heatmap of backdoor trigger. (c) Embedding change heatmap of backdoor trigger. (d) Saliency heatmap from SUM [12].

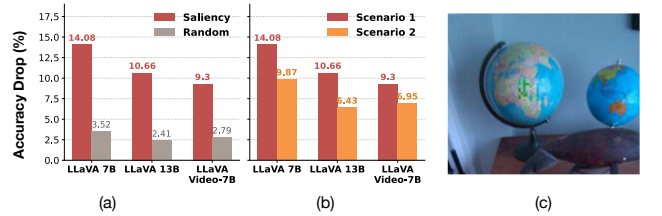


**Figure 4.** (a) The EVU accuracy drop of saliency vs. random trigger placement on EgoEverything across three models. (b) The EVU accuracy drop of attack transferability of the InvisibleHand (Scene 1) to unseen trigger variant (Scene 2) during inference across three models. (c) InvisibleHand Trigger (Scene 1).

unseen trigger patterns, thereby exhibiting trigger generalization, indicating that VLMs have good pattern memorization capability. More results on unseen triggers as well generalization to unseen trigger colors are provided in the Appendix.

#### 4.4 System Evaluation

We evaluate the real-time performance of InvisibleHand’s online stage (Section 3.3) on the Qualcomm Open-Q 865 development board [30], which integrates the Snapdragon XR2 platform powering commercial AR devices such as Ray-Neo [31] and Meta Quest [32]. Averaged over 100 frames from EgoEverything, the per-frame trigger optimization of CLIP visual encoder incurs a latency of 58 ms, within the 70 ms threshold required for a fluid AR visual experience [33]. This confirms the feasibility of executing InvisibleHand in real time on AR hardware.

## 5 Conclusion

This paper presents **InvisibleHand**, a stealthy backdoor attack targeting the visual encoder of AR-based embodied AI systems. By using imperceptible triggers and fine-tuning with only a small number of poisoned samples, InvisibleHand can map egocentric frames to attacker-chosen visual embeddings, causing the downstream VLM to reason over fabricated scenes. The results expose an underexplored security risk and highlight the need for stronger visual-encoder defenses.

## References

- [1] Y. Huang et al. VINCI: A real-time embodied smart assistant based on egocentric VLM. *arXiv:2412.21080*, 2024.
- [2] T. Tene et al. Virtual reality and augmented reality in medical education. *Frontiers in Digital Health*, 6:1365345, 2024.
- [3] G. Lampropoulos. AR, VR, and intelligent tutoring systems in education. *Applied Sciences*, 15(6):3223, 2025.
- [4] T. Gu, B. Dolan-Gavitt, and S. Garg. BadNets: Identifying vulnerabilities in the ML supply chain. *arXiv:1708.06733*, 2017.
- [5] J. Liang et al. VL-Trojan: Multimodal instruction backdoor attacks against autoregressive visual language models. *arXiv:2402.13851*, 2024.
- [6] B. Wu et al. BackdoorBench: A comprehensive benchmark of backdoor learning. *NeurIPS*, 35:10546–10559, 2022.
- [7] H. Liu, C. Li, Q. Wu, and Y. J. Lee. Visual instruction tuning. *arXiv:2304.08485*, 2023.
- [8] Q. Tang et al. EgoEverything: Long context egocentric video understanding in AR. *arXiv:2604.08342*, 2026.
- [9] T. Perrett et al. HD-EPIC: A highly-detailed egocentric video dataset. In *CVPR*, pages 23901–23913, 2025.
- [10] M. F. Aslan et al. GazeVQA: A VQA dataset for multiview eye-gaze collaborations. In *EMNLP*, pages 10481–10495, 2023.
- [11] Z. Yuan et al. BadToken: Token-level backdoor attacks to multimodal LLMs. *arXiv:2503.16023*, 2025.
- [12] A. Hosseini et al. SUM: Saliency unification through Mamba. In *WACV*, pages 1597–1607, 2025.
- [13] R. K. Mantiuk et al. FovVideoVDP: A visible difference predictor for wide field-of-view video. *arXiv:2401.11603*, 2024.
- [14] R. K. Mantiuk, M. Azimi, and A. Chapiro. ColorVideoVDP: A visible difference predictor for image, video and display distortions. *ACM TOG*, 2022.
- [15] W. Xing et al. Towards robust and secure embodied AI: A survey. *arXiv:2502.13175*, 2025.
- [16] A. Suglia et al. AlanaVLM: A multimodal embodied AI foundation model. *arXiv:2406.13807*, 2024.
- [17] A. Radford et al. Learning transferable visual models from natural language supervision. In *ICML*, 2021.
- [18] Y. Yang and M. Ren. Memory storyboard: Temporal segmentation for streaming SSL from egocentric videos. *arXiv:2501.12254*, 2025.
- [19] Y. Wang, Y. Yang, and M. Ren. Lifelong-memory: LLMs for queries in long-form egocentric videos. *arXiv:2312.05269*, 2023.
- [20] J. Bai et al. Qwen-VL: A versatile vision-language model for understanding, localization, text reading, and beyond. *arXiv:2308.12966*, 2023.
- [21] N. Carlini and A. Terzis. Poisoning and backdooring contrastive learning. In *ICLR*, 2022.
- [22] K. Grauman et al. Ego4D: Around the world in 3,000 hours of egocentric video. In *CVPR*, pages 18995–19012, 2022.
- [23] D. Damen et al. Rescaling egocentric vision: Collection, pipeline and challenges for EPIC-Kitchens-100. *TJCV*, 130(1):33–55, 2022.
- [24] S. Scholl. Comparison of embedded spaces for deep learning classification. *arXiv:2408.01767*, 2024.
- [25] Zheng et al. Universal actions for enhanced embodied foundation models In *CVPR*, 2025.
- [26] Gupta et al. Embodied intelligence via learning and evolution In *Nature communications*, 2021.
- [27] Liu et al. Embodied intelligence: A synergy of morphology, action, perception and learning In *ACM Computing Surveys*, 2025.
- [28] <https://www.meta.com/emerging-tech/orion/> Meta Orion Glass 2025.
- [29] L. Ma, J. Zhang, H. Deng, N. Zhang, Y. Liao, and H. Yu. DeCoF: Generated video detection via frame consistency. *arXiv:2402.02085*, 2024.
- [30] Lantronix, Inc. Open-Q™ 865 Development Kit for 865XR/5165RB/8250CS <https://www.lantronix.com/products/open-q-865-development-kit/>, 2025.
- [31] RayNeo RayNeo X2 AI & AR Glasses <https://www.rayneo.com/products/tcl-rayneo-x2>, 2025.
- [32] Meta Platform Inc. Meta Quest Pro <https://www.meta.com/quest/quest-pro/>, 2022.
- [33] Albert et al. Latency requirements for foveated rendering in virtual reality *ACM Transactions on Applied Perception (TAP)*, 2017.

## A Additional Experiment Results

### A.1 Saliency as the Vulnerable Point

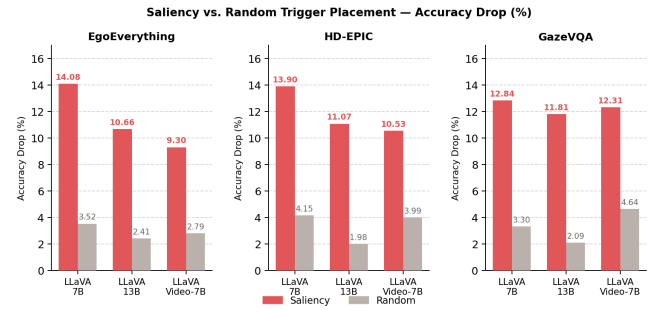


**Figure 5.** Accuracy drop (%) when placing the trigger at saliency points vs. random locations across three models and three benchmarks.

### A.2 Transferability on Unseen Trigger Colors

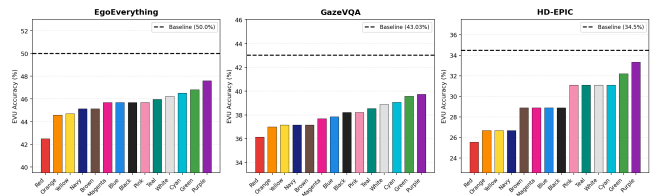


**Figure 6.** VQA accuracy of the backdoored LLaVA-13B model under 14 unseen trigger colors across EgoEverything, GazeVQA, and HD-EPIC. Dashed lines mark the clean baseline (Original Accuracy).

### A.3 Different Scenes for Transferability during Inference

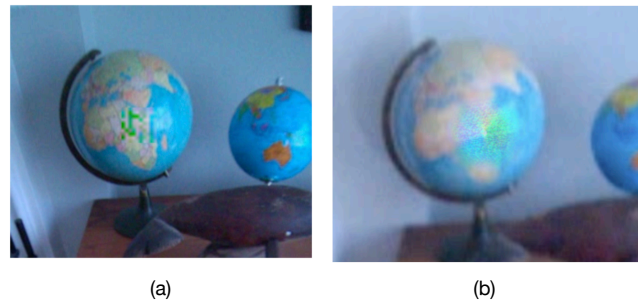


**Figure 7.** (a) Scene 1 in Figure 4b. (b) Scene 2 in Figure 4b.